Eur. Phys. J. C 35, 21–33 (2004)
Digital Object Identifier (DOI) 10.1140/epjc/s2004-01811-8

THE EUROPEAN PHYSICAL JOURNAL C

$\overline{p}p$ annihilation into four charged pions at rest and in flight

The OBELIX Collaboration

P. Salvini[1], V.I. Tretyak[2], V. Filippini[1], A. Fontana[3], P. Montagna[3], A. Panzarasa[1], A. Rotondi[3], M. Bargiotti[4], A. Bertin[4], M. Bruschi[4], M. Capponi[4], A. Carbone[4], S. De Castro[4], L. Fabbri[4], P. Faccioli[4], D. Galli[4], B. Giacobbe[4], F. Grimaldi[4], U. Marconi[4], I. Massa[4], M. Piccinini[4], N. Semprini Cesari[4], R. Spighi[4], S. Vecchi[4], M. Villa[4], A. Vitale[4], A. Zoccoli[4], A. Bianconi[5], M. Corradini[5], A. Donzella[5], E. Lodi Rizzini[5], L. Venturelli[5], A. Zenoni[6], C. Cicalò[7], A. De Falco[7], A. Masoni[7], G. Puddu[7], S. Serci[7], G. Usai[7], O.E. Gorchakov[2], S.N. Prakhov[2], A.M. Rozhdestvensky[2], M.G. Sapozhnikov[2], M. Poli[8], P. Gianotti[9], C. Guaraldo[9], A. Lanaro[9], V. Lucherini[9], C. Petrascu[9], D. Panzieri[10], F. Balestra[11], M.P. Bussa[11], L. Busso[11], P. Cerello[11], O. Denisov[11,14], L. Ferrero[11], A. Grasso[11], A. Maggiora[11], F. Tosello[11], E. Botta[12], T. Bressani[12], D. Calvo[12], F. De Mori[12], A. Feliciello[12], A. Filippi[12], S. Marcello[12], M. Agnello[13], F. Iazzi[13]

[1] INFN Sezione di Pavia, Pavia, Italy
[2] Joint Institute for Nuclear Research, Dubna, Russia
[3] Dipartimento di Fisica Nucleare e Teorica dell'Università di Pavia and INFN Sezione di Pavia, Pavia, Italy
[4] Dipartimento di Fisica dell'Università di Bologna and INFN Sezione di Bologna, Bologna, Italy
[5] Dipartimento di Chimica e Fisica per l'Ingegneria e per i Materiali, Università di Brescia, Brescia, Italy and INFN gruppo collegato di Brescia, Brescia, Italy
[6] Dipartimento di Meccanica, Università di Brescia, Brescia, Italy and INFN Sezione di Pavia, Pavia, Italy
[7] Dipartimento di Scienze Fisiche, Università di Cagliari and INFN Sezione di Cagliari, Cagliari, Italy
[8] Dipartimento di Energetica dell'Università di Firenze, Firenze, Italy and INFN Sezione di Bologna, Bologna, Italy
[9] Lab. Naz. di Frascati dell'INFN, Frascati, Italy
[10] Dipartimento di Scienze e Tecnologie Avanzate, Università del Piemonte Orientale and INFN Sezione di Torino, Torino, Italy
[11] Dipartimento di Fisica Generale "A. Avogardo" dell'Università di Torino and INFN Sezione di Torino, Torino, Italy
[12] Dipartimento di Fisica Sperimentale dell'Università di Torino and INFN Sezione di Torino, Torino, Italy
[13] Dipartimento di Fisica del Politecnico di Torino and INFN Sezione di Torino, Torino, Italy
[14] on leave ob absence from Joint Institute for Nuclear Research, Dubna, Russia

Received: 2 December 2003 /
Published online: 23 April 2004 –

Abstract. The spin-parity analysis of the data on the $\bar{p}p \to 2\pi^+ 2\pi^-$ annihilation reaction at rest in liquid and in gaseous hydrogen at 3 bar pressure and in flight at $\overline{p}$ momentum of $\simeq 50$ MeV/c, collected by the Obelix spectrometer at the LEAR complex of CERN, is presented. The relative branching ratios $(a_1(1260) \to \sigma\pi)/(a_1(1260) \to \rho\pi) = 0.06 \pm 0.05$ and $(\pi(1300) \to \sigma\pi)/(\pi(1300) \to \rho\pi) = 2.2 \pm 0.4$ are obtained. It is also shown that the inclusion of the exotic meson $\pi_1(1400)$, $J^{PC} = 1^{-+}$, mass and width $M = 1.384 \pm 0.028$, $\Gamma = 0.378 \pm 0.058$ GeV/c^2, in its decay to $\rho\pi$, improves the fit and some implications of these results are briefly discussed. The relative S and P-wave annihilation percentages in four charged pions at two target densities are obtained.

1 Introduction

One of the most interesting aspects of the

$$\bar{p}p \to 2\pi^+ 2\pi^- \tag{1}$$

annihilation at low energy is the possibility of producing many light mesons, according to the list of Table 1.

The first analysis of the reaction (1) goes back to about 30 years ago, when Diaz et al. [1] analyzed 6 665 annihilations at rest in a liquid hydrogen (LH2) bubble chamber. A satisfactory fit was achieved by considering the production of what presently are called the $\rho(770)$, $a_1(1260)$, $f_2(1270)$ and $a_2(1320)$ mesons, together with a $\pi\pi$ S-wave with poles at 0.8 and 1.1 GeV/c^2 and a zero at 0.94 GeV/c^2. The spin-parity analysis was performed by assuming only $^1S_0$ and $^3S_1$ $\bar{p}p$ protonium initial states. However, from the ensemble of the existing data on $\overline{p}p$ annihilations at rest now it turns out that the percentage of protonium annihilations in P-waves in liquid is larger than 10% [2–4]. We note that the inclusion of the four P-waves of Table 1 makes the analysis difficult, because the intermediate states produced by the annihilation contain many large-width resonances that overlap or interfere each other.

Table 1. Possible intermediate states (channels) in the $\bar{p}p \to 2\pi^+ 2\pi^-$ reaction (notations are from (5) and (6)). The exotic state 1^{-+} is indicated as π_1, σ stands for the $(\pi\pi)$ S-wave interaction and ρ' for the $\rho(1450)$ meson. Only the lowest angular momenta L are considered

$\bar{p}p$	channel	I	L	l_1	l_2	$\bar{p}p$	channel	I	L	l_1	l_2
$^1S_0$	$\rho\,\rho$	0	1	1	1	$^3P_0$	$\sigma\,\sigma$	0	0	0	0
	$a_2(1320)\,\pi$	0	2	2	1		$\rho\,\rho$	0	0	1	1
	$\pi_1\,\pi$	0	1	1	1		$\sigma\,f_2(1270)$	0	2	0	2
$^3S_1$	$\rho\,\sigma$	1	0,2	1	0		$a_1(1260)\,\pi$	0	1	0	1
	$\rho'\,\sigma$	1	0,2	1	0		$[\pi(1300)]_{\sigma\pi}\pi$	0	0	0	0
	$\rho\,f_2(1270)$	1	0	1	2		$[\pi(1300)]_{\rho\pi}\pi$	0	0	1	1
	$a_1(1260)\,\pi$	1	0	0	1	$^3P_1$	$\rho\,\rho$	0	0	1	1
	$a_2(1320)\,\pi$	1	2	2	1		$a_1(1320)\,\pi$	0	1	0	1
	$[\pi(1300)]_{\sigma\pi}\,\pi$	1	1	0	0		$a_2(1320)\,\pi$	0	1	2	1
	$[\pi(1300)]_{\rho\pi}\,\pi$	1	1	1	1		$\sigma\,f_2(1270)$	0	2	0	2
	$\pi_1\pi$	1	1	1	1		$\pi_1\,\pi$	0	0	1	1
$^1P_1$	$\rho\,\sigma$	1	1	1	0	$^3P_2$	$\rho\,\rho$	0	0	1	1
	$a_1(1260)\,\pi$	1	1	0	1		$\sigma\,\sigma$	0	2	0	0
	$a_2(1320)\pi$	1	1	2	1		$a_1(1260)\,\pi$	0	1	0	1
	$\rho\,f_2(1270)$	1	1	1	2		$a_2(1320)\,\pi$	0	1	2	1
	$\pi_1\pi$	1	0	1	1		$\sigma\,f_2(1270)$	0	0	0	2
							$[\pi(1300)]_{\sigma\pi}\pi$	0	2	0	0
							$[\pi(1300)]_{\rho\pi}\pi$	0	2	1	1

To overcome this difficulty, we decided to study the reaction (1) in flight with low momentum $\bar{p}$ and at rest with targets of different density. The annihilation in flight at very low momentum proceeds mainly from S-wave, with a P-wave contribution of about 4%, for a $\bar{p}$ momentum of about 50 MeV/c [5–7]. On the contrary, the annihilation at rest takes place after the electromagnetic cascade of the antiprotonic atom and the percentage of annihilations from the S and P-atomic states varies with the target density [2–4]. In this way the mixture of the six $\bar{p}p$ partial waves or initial states is changed, together with the corresponding meson production from the intermediate states. In principle, the combined spin-parity analysis of these data should help to disentangle the contributions of the various mesons.

In 1997 our Collaboration published the spin-parity analysis of a sample of 31157 annihilation events taken in flight at very low $\bar{p}$ incident momentum ($\simeq$ 50 MeV/c) [8]. The best fit solution required also the presence of a $\rho(1450)$ state and of a heavy pion $\pi(1300)$. However, these contributions were small and only the S-wave was considered, omitting the 4% of P-wave contribution.

This study continued with the combined analysis of two samples obtained from the annihilation at rest in gaseous and in liquid hydrogen (LH2) targets [9] and with the very preliminary analysis of all the three samples [10].

Here we present the final results of the spin-parity analysis of these three samples, obtained through the continuous refinement of our algorithms and models of the amplitude (see Sect. 3) and with the inclusion in Table 1 of a set of intermediate states more complete than that considered in [10].

One of the points of our investigation is the system $(\pi^+\pi^-)$ with the two pions in relative S and P waves.

The $\pi\pi$ isoscalar S-wave, known in the past as the σ meson or the σ interaction (and noted in this way in Table 1), has been studied extensively during the last decades. An updated reanalysis of the topic can be found in [11], where a full set of references to earlier works is also given. At present, this wave is parametrized as the coherent sum of four poles: the broad $f_0(600)$ (now called the σ, $\Gamma \simeq 600$ MeV), the narrow $f_0(980)$ ($\Gamma \simeq 50$ MeV), the broad $f_0(1370)$ ($\Gamma \simeq 300$ MeV) and the narrow $f_0(1500)$ ($\Gamma \simeq 100$ MeV). In the previous work [8] we verified that the data in flight were compatible with a three pole S-wave; here in Sect. 3 we check this point by fitting the three data samples, comparing this result also with that obtained with some recent four pole amplitudes.

For what concerns the $(\pi^+\pi^-)$ P-wave, in addition to the huge $\rho(770)$ signal, there is some uncertainty about the parameters of the $\rho(1450)$ and $\rho(1700)$ radial excitations [8, 11]. In our case we considered only the lower mass $\rho(1450)$ case, listed as ρ' in Table 1. Here we investigate further the influence of the ρ' mass on our best fit solution, since in our previous analysis we found a mass lower than that quoted in the Particle Data Group (PDG) [8].

Another important reason for our interest in the $\bar{p}p \to 2\pi^+\,2\pi^-$ channel concerns the exotic meson $\pi_1(1400)$ with

quantum numbers $J^{PC} = 1^{-+}$, $I = 1$, which is a candidate for a hybrid meson or a multiquark state, with quantum numbers not accessible to the $\bar{q}q$ system. The evidence of its existence comes from two different experiments that analysed the decay mode into $\eta\pi$ [12–15].

In these data we search for this meson by analyzing the $\pi_1 \to \rho\pi$ decays, that are allowed from the $^1S_0$, $^3S_1$, $^1P_1$ and $^3P_1$ states. For the first time we consider here also the π_1 production from S-states and perform a grid search to find the best fit mass and width values.

Finally, we consider also the $\pi(1300)$ meson (indicated also as π') production and its decay branching ratio into $\rho\pi$ and $\sigma\pi$, which is still not very well known experimentally (theoretical predictions can be found, for example, in [16]).

The amplitude obtained taking into account all these physics aspects and the intermediate states of Table 1 gives much better χ^2 values than in [10]. The results will be discussed in detail in Sect. 4.

2 Event selection

We consider a total of 90 000 annihilation events from reaction 1, divided into three different data sets, each one with $\simeq$ 30 000 annihilation events, obtained at rest on a LH2 target, at rest on a gaseous hydrogen target (at 3 bar pressure) and in flight at very low incident antiproton momentum (around 50 MeV/c).

The data were taken until the end of 1996 with the Obelix spectrometer at the Low Energy Antiproton Ring at CERN.

The whole apparatus was immersed in a magnetic field, reaching the maximum value of $\simeq 0.5$ T along its axis. In order to optimize the number of the annihilation events, the inner part of the apparatus was different for the different data samples. For the annihilation events at rest in the gaseous hydrogen target and in flight at low momentum, a 20 cm radius and $\simeq$ 50 cm length cylindrical target has been used, containing gaseous hydrogen at 3 bar (at rest data) or 0.8 bar (in flight data) pressure. A detailed explanation of the experimental layout and of the in-flight annihilation selection is given in [17,18]. For the annihilation events at rest in LH2 the target was the same used for the $\bar{n}$ data taking [19].

The targets were surrounded by a first layer of 30 thin (1 cm) plastic scintillators, arranged in a barrel and providing the start for the time of flight system (TOF). The incident antiprotons were selected by requiring the coincidence of the signals of the beam scintillator and this scintillator barrel. The outer scintillator barrel (90 elements, $9\times4\times350$ cm^3 each) allowed the first level trigger on multiplicities and on particle identification. A Jet Drift Chamber (JDC), placed between the two scintillator barrels, was devoted to the tracking of charged particles, with a momentum resolution of $\sim$ 2% for pions around 300 MeV/c [20]. The JDC allowed the determination of the annihilation vertex and contributed with the TOF to the identification of the event topology and to the particle identification through the $\mathrm{d}E/\mathrm{d}x$ measurement.

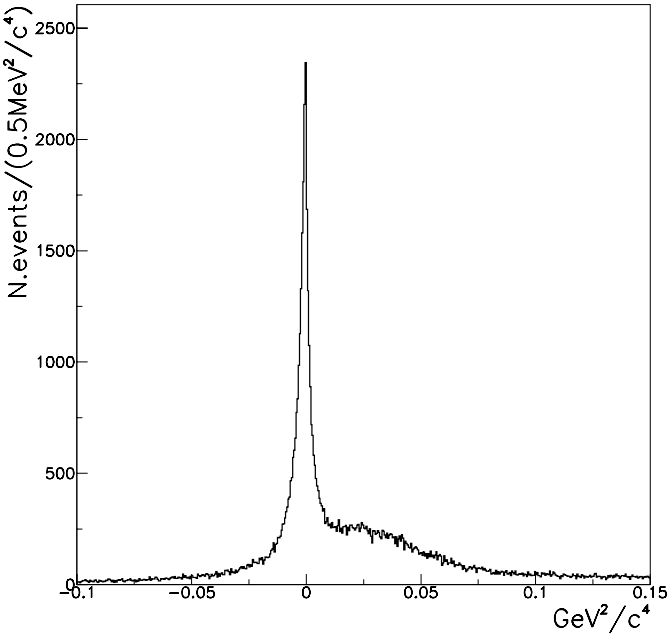

Fig. 1. Missing mass squared distribution of the 4-prong events that pass the selection criteria described in the text. The peak corresponds to the $\bar{p}p \to 2\pi^+2\pi^-$ channel, the shoulder at its right contains mostly $\bar{p}p \to 2\pi^+2\pi^-\,\pi^0$ events, whereas the underlying flat background comes mainly from the $\bar{p}p \to \pi^+\pi^-\,2\pi^0$ reaction

The complete description of the apparatus can be found in [21].

For each data set we collected about $4\,10^6$ annihilation events with a four prong TOF multiplicity trigger. About one tenth of these events($\simeq 3.5\,10^5$) passed the following "4-prong" selection criteria:

- four tracks successfully connected to the vertex into the fiducial target volume;
- zero total charge;
- track lengths > 20 cm, to have a momentum resolution $< 2\%$ [20].

The typical missing mass distribution (for in flight annihilation) of the 4-prong events obtained with this selection procedure is shown in Fig. 1. Finally, the $\bar{p}p \to 2\pi^+2\pi^-$ events were extracted from the 4-prong sets by applying a four-constraint kinematical fit with 95% C.L. At the end of the selection, the three final data sets had $\simeq$ 30 000 events each. All this procedure was carefully repeated with the Obelix Monte Carlo code, and the resulting background contamination resulted less than 1%.

The contamination from the $\bar{p}p \to K^0_S K^0_S \to 2\pi^+2\pi^-$ reaction is negligible, since the $K^0_S K^0_S$ intermediate state is forbidden from S-wave initial states, so that the measured frequency in LH2 is consistent with zero ($(4 \pm 3)\,10^{-6}$, from [22, 23]) and in a NTP gas target is very low ($(3 \pm 1)\,10^{-5}$, from [24]). Comparing this last value with the frequency (4) and taking into account the $K^0_S \to \pi^+\pi^-$ branching ratio, one obtains an upper limit contamination of 7 $K^0_S K^0_S$ events in a sample of 30 000 events.

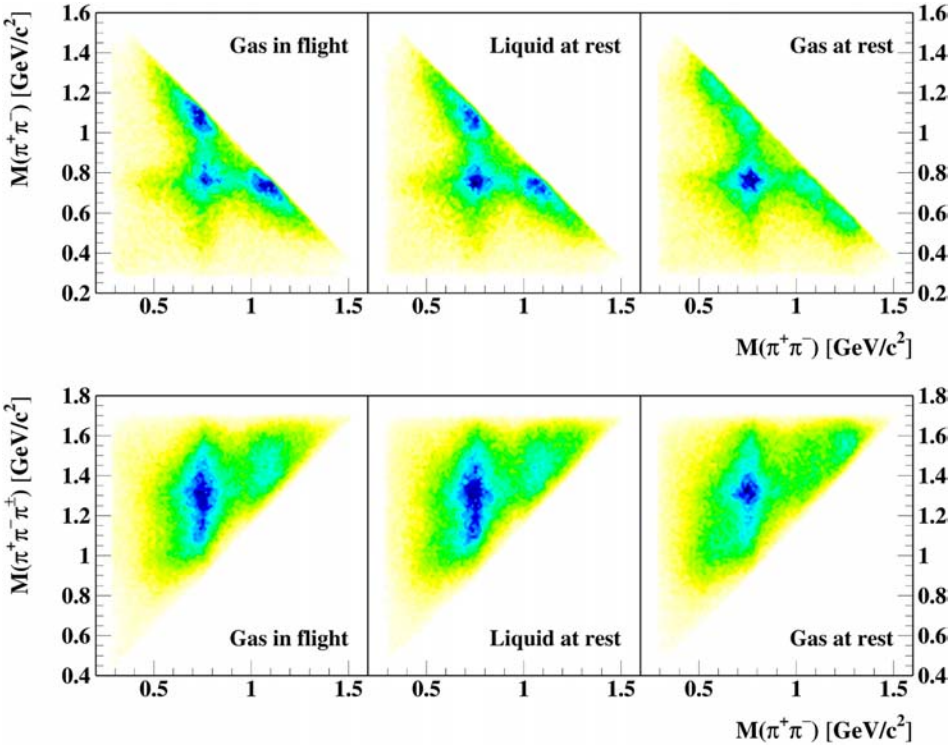

Fig. 2. Bidimensional invariant mass distributions for $\bar{p}p \to 2\pi^+2\pi^-$ experimental data taken in hydrogen targets at three different conditions. The number of combinations per event is 4 for $M(\pi_a^+\pi_b^-)$ versus $M(\pi_c^+\pi_d^-)$ (top) and 8 for $M(\pi_a^+\pi_b^-\pi_c^\pm)$ versus $M(\pi_a^+\pi_b^-)$ (bottom)

The $\bar{p}p \to 2\pi^+2\pi^-$ reaction branching ratios have been previously measured and are:

$$B_{4\pi}(\text{in flight}) = (7.61 \pm 0.35)\,10^{-2}\ , \tag{2}$$

$$B_{4\pi}(\text{liquid}) = (6.00 \pm 0.24)\,10^{-2}\ , \tag{3}$$

$$B_{4\pi}(\text{NTP gas}) = (6.4 \pm 0.9)\,10^{-2}\ , \tag{4}$$

where the value (2) comes from our previous analysis of the in flight data [8], the value (3) is the weighted average of the values at rest in LH2 $(6.9\pm0.6)\,10^{-2}$ [1], $(5.8\pm0.3)\,10^{-2}$ [22], $(5.9 \pm 0.5)\,10^{-2}$ [23] and the last value (4) comes from the annihilations at rest in gaseous hydrogen at NTP of [24].

We assume in the following that the NTP gas value is a good estimate also for our 3 bar gas target in spite of the different target pressures, because the interpolation of the P-wave percentages between 1 and 15 bar target pressures shows that the branching ratios taken at 3 bar target pressure can differ from the NTP ones by no more than 5% [2,25].

As discussed before, the three data sets are expected to be very different for what concerns the mixture of partial waves involved in the $\bar{p}p$ annihilation.

This behaviour is confirmed by our data, as reported in Figs. 2 and 3. In the $\pi^+\pi^-$ scatter plots of Fig. 2 a strong $\rho\rho$ signal is present in each sample; a system made by a ρ recoiling against a $\pi\pi$ couple (the σ) with an energy around 1.1 GeV is also evident in the in flight and liquid target samples, that is in association with a high fraction of S-waves. Figures 3a, b, and c show clearly that the production of the $f_2(1270)$ meson increases with P-wave. Finally, the scatter plot of the three pion invariant mass versus the two pion one of Fig. 2 and the spectra d, e, and f of Fig. 3 show a clear $a_2(1320)$ production, associated to a more complicated dynamics.

3 The amplitude

We assume that the amplitude for the $\bar{p}p$ annihilation into four pions is well described taking into account the two following decay chains :

$$\bar{p}p \to [AB]_L \to [(\pi\pi)_{l_1}(\pi\pi)_{l_2}]_L \tag{5}$$

$$\bar{p}p \to [A\pi]_L \to \left[\,[B\pi]_{l_1}\,\pi\,\right]_L \to \left[\,[(\pi\pi)_{l_2}\pi]_{l_1}\pi\,\right]_L \tag{6}$$

where A and B are resonant states and L, l_1, l_2 are the two particle orbital angular momentum quantum numbers. The possible intermediate states (channels) are summarized in Table 1.

The decay intensity $\mathcal{J}$ for the annihilation at rest can be written as an incoherent sum over the six lowest $\bar{p}p$ atomic states of Table 1 with J^{PC} (or $^{2S+1}L_J$) fixed quantum numbers. Indicating with the index J these atomic states we can write:

$$\mathcal{J}(q_1,q_2,q_3,q_4) = \sum_J \mid \mathbf{A}_J \mid^2 \quad \text{where} \tag{7}$$

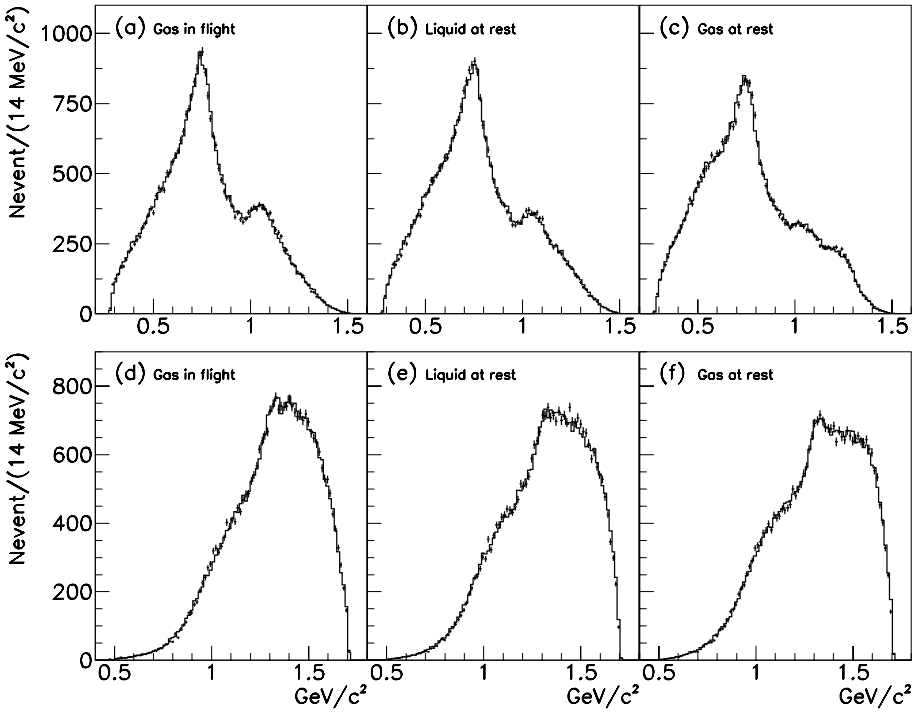

Fig. 3. Comparison between experimental data (points with error bars) and theoretical amplitude (histogram) from fit D. **a**, **b**, **c**: $M(\pi^+\pi^-)$, **d**, **e**, **f**: $M(\pi^+\pi^-\pi^\pm)$ respectively for the three different data sets. The number of combinations per event is 4 for all the plots

$$\mathbf{A}_J = \sum_{Ikp} [a_{Jk}\, C_I\, \mathbf{Z}_{Jk}(\mathbf{q})\, F_k(q)]_p \equiv \sum_k a_{Jk} \sum_{Ip} \mathcal{F}_{Ikp} \ ,$$

where q_i, $i = 1, 2, \ldots, 4$ are the four-momenta of the final pions, C_{Ik} are the isospin coefficients, a_{Jk} are the complex parameters to be fitted, $\sum_p$ stays for the permutations over identical particles, $k \equiv (L, l_1, l_2)$ identifies the set of quantum numbers of the states listed in Table 1, $\mathbf{Z}_{Jk}(\mathbf{q})$ are the spin functions, F describes the energy behaviour of the decay chain and $\mathbf{q}$ denotes the set of break-up momenta of the intermediate states of the reaction. The normalization is such that $|a_{Jk}|^2$ represents the fraction of events due to the corresponding $\mathcal{F}_{Ikp}$ isobar amplitude, ignoring the interference terms.

The decay intensity for the in-flight annihilation events is written as an incoherent sum over the four possible $(\lambda_p, -\lambda_{\overline{p}})$ helicity states of the $\overline{p}p$ system, corresponding to the three spin component values $M_J = 0, \pm 1$:

$$\mathcal{J}(q_1, q_2, q_3, q_4) = \sum_{\lambda_p, \lambda_{\overline{p}}} |\ \mathbf{A}_{\lambda_p \lambda_{\overline{p}}}\ |^2 \qquad \text{where} \tag{8}$$

$$A_{\lambda_p, \lambda_{\overline{p}}} = \sum_{IJp} [a_{J,\lambda_p \lambda_{\overline{p}} k}\, C_I\, \mathbf{Z}_{J,\lambda_p\, \lambda_{\overline{p}}\, k}(\mathbf{q})\, F_{\lambda_p \lambda_{\overline{p}} k}(q)]_p \ .$$

We note that in (7) states with different $J \equiv J^{PC}$ add incoherently because they are in principle distinguishable (as the protonium cascade X-rays are observable), whereas in (8) the states with different J^{PC} values interfere [26].

Since in (7) the complex coefficients a_{Jk} parametrize the isobar decay probability from a certain J^{PC} state, one usually assumes $a_J \equiv a_{JM}$, $|M| \leq J$, so that any term $a_{J\lambda_p\lambda_{\overline{p}}}$ in (8) corresponds to a term a_{JM} with $M = 0, \pm 1$. In this way, for the in flight data the free parameters are a subset of the a_J coefficients of the at rest amplitude, and the connection between the in flight and at rest amplitudes is assured during the fit.

The spin functions $\mathbf{Z}$ are written in terms of the covariant Zemach tensors in the formulation of [27], extending the formalism to the case of the $(\rho\rho)_l$ system in a relative angular momentum $l = 1$ (see the Appendix). All these tensors give the same spin amplitudes of the covariant helicity formalism of [28].

As in our previous paper [8], the complex functions $F_k(q)$ describe the energy-dependent part of the amplitudes. In most of the cases of Table 1 they are written as a product of Breit-Wigner functions describing the resonances present in the decay chain, parametrized as in [29,30]:

$$F(q) = \frac{1}{(qR)^l}\, W_l(q)\, \frac{m_0 \Gamma_0}{m_0^2 - m^2 - i\, m_0 \Gamma(m)} \tag{9}$$

$$\Gamma(m) = \Gamma_0\, \frac{m_0}{m}\, \frac{q}{q_0}\, \frac{W_l^2(q)}{W_l^2(q_0)}$$

where $R = 1$ fm (a typical value [30]), q_0 is the break-up momentum calculated at the resonance mass value, l is the relative angular momentum of the resonance decay products, and W_l are the Blatt-Weisskopf centrifugal barrier factors. The first three coefficients with $l = 0, 1, 2$, are:

$$W_0(q) = 1 \ ,$$

$$W_1(q) = qR\left[\frac{2}{1+(qR)^2}\right]^{1/2}, \quad (10)$$

$$W_2(q) = (qR)^2\left[\frac{13}{9+3(qR)^2+(qR)^4}\right]^{1/2}.$$

The factor $1/(qR)^l$ multiplying the Breit-Wigner function eliminates the terms $(qR)^l$ in (10), since they are already present in the covariant Zemach tensors. On the contrary, this correction is absent in the definition of the widths $\Gamma(m)$.

The break-up momenta $q(m)$ for the decays into two pions are calculated as $q(m) = m\sqrt{1-(4m_\pi^2/m^2)}/2$ and the two-body phase space is given by $\rho(m) = 2q(m)/m$.

In the case of quasi two-body decays to describe the partial width mass dependence we evaluate the phase space factor integrating the squared decay amplitude over the three-pion phase space available Φ_3

$$\rho_j(m) = \int |A_j|^2 d\Phi_3, \quad (11)$$

where A is the decay amplitude of $a_1(1260)$, $a_2(1320)$, $\pi(1300)$ or π_1 and $j = (\rho\pi)$, $(\sigma\pi)$ stands for the decay mode. For instance to describe the spin-0 resonance decays $\pi(1300) \to \sigma\pi$, $\pi(1300) \to \rho\pi$, with nominal mass and width m_0 and Γ_0 and the coupling coefficients $\gamma_j^2 = (\Gamma_j/\Gamma_0)/\rho_j(m_0)$, we use the Breit-Wigner function [29,31]:

$$[F_k(\mathbf{q})]_j = \frac{m_0\Gamma_0\gamma_j}{m_0^2 - m^2 - i\, m_0\Gamma_{\rm tot}(m)}, \quad (12)$$

with partial and total widths given by:

$$\Gamma_j(m) = \Gamma_0\,\gamma_j^2\rho_j(m) \quad (13)$$
$$\Gamma_{\rm tot}(m) = \sum_j \Gamma_j(m).$$

The decay branching ratio is defined in this case as:

$$\frac{\Gamma(\pi' \to \sigma\pi)}{\Gamma(\pi' \to \rho\pi)} = \frac{\gamma^2_{\pi'\to\sigma\pi}\rho_{\pi'\to\sigma\pi}(m_0)}{\gamma^2_{\pi'\to\rho\pi}\rho_{\pi'\to\rho\pi}(m_0)} \quad (14)$$

As in our previous paper [8], the function F_k of (7), for the case of the $\pi\pi$ S-wave interaction (the σ term in Table 1), is parametrized in terms of the K-matrix formalism [29]. Following the N/D method, it is possible to write the σ interaction in the form [32]:

$$F_k = \frac{(\Lambda_1+\Lambda_2 s)K_{11} + i\rho_2\Lambda_3(K_{11}K_{22}-K_{12}^2)}{1-i\rho_1K_{11}-i\rho_2K_{22}-\rho_1\rho_2(K_{11}K_{22}-K_{12}^2)} \quad (15)$$

where s is the invariant mass squared of the $\pi\pi$ system, and ρ_1 and ρ_2 are the two-body phase space factors for the decay into $\pi\pi$ and $K\bar{K}$. The Λ production complex parameters are different for each of the six initial $\bar{p}p$ states of Table 1 and are left free during the fit when σ is produced in $\bar{p}p$ annihilation. For the σ produced by the resonance decays, we use the Λ parameters fixed at $\Lambda_1 = 1$, $\Lambda_2 = 0$, $\Lambda_3 = -1$, corresponding to the usual K-matrix scattering theory [29].

During the data analysis described below, we compared the N/D approach to the P-vector one [29] and verified that the two parametrizations give consistent results, as in [33].

Finally, we treat the overlap of the ρ and $\rho\prime$ resonances, which have the same spin-parity and the same partial waves, by writing the function F_k of (7, 8) as a 1×1 K-matrix [29]:

$$F_k(m) = [1 - i\rho(m)K_{\rho\rho'}]^{-1}\,P_{\rho\rho'}, \quad (16)$$

where

$$K_{\rho\rho'} = \sum_{j=1}^{2}\frac{m_i\Gamma_j}{\rho(m_j)}\left[\frac{W_1(q)}{W_1(q_j)}\right]^2\frac{1}{m_j^2-m^2}$$

$$P_{\rho\rho'} = \sum_{j=1}^{2}\beta_j\sqrt{\frac{m_j\Gamma_j}{\rho(m_j)}}\left[\frac{W_1(q)}{W_1(q_j)}\right]\left(\frac{q_j}{q_{0j}}\right)\frac{1}{m_j^2-m^2}$$

and $m_j, \Gamma_j, \rho(m_j)$ and q_j are mass, width, two-body phase space factor and break-up momentum of the two ρ's. The factor W_1 is defined in (10). We drop also in this case, by multiplying by (q_j/q), the factor q from the P-vector, because it is already present in the Zemach tensors. The complex production parameters β_j are left free during the fit.

The data have been fitted with the maximum likelihood method. Using the Minuit program [34] we minimize the quantity $-\ln(\mathcal{L}_{\rm tot})$, where $\mathcal{L}_{tot}$ is the total likelihood $\mathcal{L}_{\rm tot} = \mathcal{L}_{\rm flight}\,\mathcal{L}_{\rm liquid}\,\mathcal{L}_{\rm gas}$. On each data set, the likelihood is computed as

$$\mathcal{L} = \prod_{j=1}^{N_{\rm ev}}\mathcal{J}_j \Big/ \left(\sum \mathcal{J}_{MC}\right), \quad (17)$$

where $N_{\rm ev}$=30 000, $\mathcal{J}_j$ is the event by event decay probability of (7) and (8) and the denominator is the likelihood normalization, evaluated (for each data sample) over a set of 90 000 Monte Carlo events.

The annihilation fractions from one of the six $\bar{p}p$ initial states J are defined from the a_{JK} coefficients of (7) as:

$$P_J = \frac{\sum_k |a_{Jk}|^2}{\sum_{Jk}|a_{Jk}|^2}. \quad (18)$$

These fractions can be multiplied by the branching ratio (2–4), giving the $\bar{p}p \to 2\pi^+2\pi^-$ branching ratio from the state J, that usually is written in the form [2–4]:

$$P_J(\delta)\,B_{4\pi}(\delta) = f_J(\delta)\,E_J(\delta)\,g_J B_J, \quad (19)$$

where the explicit dependence of the terms on the target density δ has been put in evidence. Here f_J is the S-wave (or P-wave) fraction in the case of the $^1S_0$, $^3S_1$ (or $^1P_1$ $^3P_0$ $^3P_1$ $^3P_2$) states, E_J is the enhancement factor that is equal to one when the population of the J state follows the spin statistics, g_J is the known spin statistical weight and B_J is the density independent hadronic branching ratio $\bar{p}p \to 2\pi^+2\pi^-$ from the J channel.

Table 2. Results of fit A (see the text). The decay fractions are normalized to 100 for each $\overline{p}p$ state, whose relative weight within the S and P-waves is also given. The π' indicates the $\pi(1300)$ pion and σ the $(\pi\pi)$ S-wave interaction. Some of the channels of Table 1, suppressed for dynamical reasons and refused by the fit, are omitted here. The interference terms for the amplitude of (8) are very different from those of (7), so for the in-flight data we give only the total P-wave percentage. The $\chi^2$is the *pseudo*-χ^2 per bin calculated over a set of 15 histograms (see the text)

$\overline{p}p$	channel	LH2 and gas	$\overline{p}p$	channel	LH2 and gas
$^1S_0$	all	24.5 ± 0.5	$^3P_0$	all	25.4 ± 0.9
$^3S_1$	all	75.5 ± 0.5	$^3P_1$	all	9.4 ± 1.0
$^1P_1$	all	7.6 ± 1.3	$^3P_2$	all	57.6 ± 1.2
$^1S_0$	$\rho\rho$	31.8 ± 0.9	$^3P_0$	$\sigma\sigma$	60.5 ± 1.5
	$a_2\pi$	68.2 ± 0.9		$\rho\rho$	16.9 ± 1.2
$^3S_1$	$\rho\sigma$	53.4 ± 0.6		σf_2	8.7 ± 1.0
	ρf_2	23.0 ± 0.5		$a_1\pi$	12.3 ± 1.2
	$a_1\pi$	18.0 ± 0.5		$\pi'\pi$	1.6 ± 0.6
	$a_2\pi$	2.3 ± 0.2	$^3P_1$	$\rho\rho$	36.2 ± 3.4
	$\pi'\pi$	3.3 ± 0.3		σf_2	23.7 ± 4.1
$^1P_1$	$\rho\sigma$	56.5 ± 4.0		$a_1\pi$	10.1 ± 3.4
	ρf_2	10.3 ± 0.7		$a_2\pi$	30.0 ± 6.2
	$a_1\pi$	0.7 ± 0.2	$^3P_2$	$\sigma\sigma$	2.4 ± 0.4
	$a_2\pi$	32.5 ± 4.8		σf_2	48.3 ± 1.3
				$a_1\pi$	25.1 ± 1.3
				$a_2\pi$	20.2 ± 1.0
				$\pi'\pi$	4.0 ± 0.8

P-wave percentages				χ^2		
flight	LH2	gas	$2\ln\mathcal{L}_{TOT}$	flight	LH2	gas
10.2 ± 0.9	28.2 ± 0.8	64.6 ± 0.9	61758	1.3	1.3	1.3

4 Results

The most important fits will be referred to as follows:

A) All the channels from Table 1 are considered, except those concerning the π_1 (1^{-+}) production. The annihilation fractions defined in (18), (19) from S and P-waves (different L states) vary with the target pressure, but the atomic S and P-sublevel fractions are the same in liquid and at 3 bar hydrogen target pressure.
B) The same channels as in fit A are included. The annihilation fractions from atomic sublevels can vary freely as a function of the target pressure.
C) Same as fit A, but with the π_1 production.
D) Same as fit B, but with the π_1 production.

The different fits are obtained by minimizing the log likelihood (17) and can be also qualitatively compared on the basis of a χ^2 per bin from a set of 15 histograms, empirically chosen to give a χ^2 tracking adequately the log likelihood changes and assuming a value $\simeq 1$ over a set of Monte Carlo data when the right amplitude is used. However, in some cases, in the vicinity of the best fit solution, this χ^2 behaves as an inconsistent estimator, remaining more or less constant also when significant changes in the log likelihood are observed. For these reasons in the following we will refer to this quantity as the *pseudo*-χ^2.

In Figs. 3 some of the histograms of the previously mentioned set are shown. In Tables 2 and 3 the results from fits A and D are presented.

The $(\pi\pi)$ S, P and D-waves considered in the fit are listed in Table 1.

The more complicated is the $(\pi\pi)$ S-wave (indicated as σ in Tables 1, 2 and 3) since in the energy region available four resonant states are present: the very broad $f_0(400–1200)$, the $f_0(980)$, $f_0(1370)$ and $f_0(1500)$. The spin-parity fit has been performed using different forms for the $(\pi\pi)$ S-wave: a 4-pole K-matrix from [35] and a 3-pole K-matrix from [36], using (15) and the N/D method [32]. We stress that, in the case of 3-pole K-matrix, the N/D method is equivalent to the production vector approach, as both introduce three complex parameters (for each initial state) in the fit and it is possible to write the analytical relations between the parameters in the two approaches. On the contrary, the use of the 4-pole $(\pi\pi)$ S-wave in the P-vector frame introduces four complex parameters: one more than the N/D approach. Despite the different number of fit parameters, the two

Table 3. Results of fit D and percentages of the intermediate states. Description as in Table 2, only the % of atomic sublevels are different for annihilation in gas (3 bar pressure) and in liquid

$\overline{p}p$	channel	LH2	gas	$\overline{p}p$	channel	LH2	gas
$^1S_0$	all	25.3 ± 0.7	23.4 ± 1.2	$^3P_0$	all	41.2 ± 1.8	23.8 ± 0.9
$^3S_1$	all	74.7 ± 0.7	76.6 ± 1.2	$^3P_1$	all	15.6 ± 1.6	8.2 ± 0.8
$^1P_1$	all	3.2 ± 1.5	9.6 ± 0.8	$^3P_2$	all	40.0 ± 2.3	58.4 ± 1.1
$^1S_0$	$\rho\rho$	33.1 ± 0.8		$^3P_0$	$\sigma\sigma$	56.0 ± 1.4	
	$a_2\pi$	58.4 ± 2.0			$\rho\rho$	16.3 ± 2.5	
	$\pi_1\pi$	8.5 ± 1.8			σf_2	8.7 ± 0.9	
$^3S_1$	$\rho\sigma$	52.0 ± 0.7			$a_1\pi$	15.6 ± 1.5	
	ρf_2	24.6 ± 0.5			$\pi'\pi$	3.4 ± 0.7	
	$a_1\pi$	17.8 ± 0.5		$^3P_1$	$\rho\rho$	34.1 ± 0.7	
	$a_2\pi$	1.9 ± 0.2			σf_2	16.2 ± 3.0	
	$\pi'\pi$	2.8 ± 0.2			$a_1\pi$	0.6 ± 0.6	
	$\pi_1\pi$	0.9 ± 0.1			$a_2\pi$	2.0 ± 2.0	
$^1P_1$	$\rho\sigma$	42.5 ± 4.4			$\pi_1\pi$	47.1 ± 5.2	
	ρf_2	14.8 ± 3.8		$^3P_2$	$\sigma\sigma$	2.1 ± 0.4	
	$a_1\pi$	4.3 ± 1.9			σf_2	51.6 ± 1.0	
	$a_2\pi$	34.7 ± 5.2			$a_1\pi$	22.3 ± 1.3	
	$\pi_1\pi$	3.7 ± 2.0			$a_2\pi$	20.4 ± 0.9	
					$\pi'\pi$	3.6 ± 0.7	

P-wave percentages				χ^2		
flight	LH2	gas	$2 \ln \mathcal{L}_{TOT}$	flight	LH2	gas
10.3 ± 0.9	27.8 ± 0.8	63.5 ± 0.9	62240	1.2	1.2	1.2

different $(\pi\pi)$ S-waves in the two approaches give similar results, both for histogram shape and likelihood values: the fact can be explained taking into account that in our channel only the low-energy part of the $(\pi\pi)$ S-wave is important, which is very similar for the two $(\pi\pi)$ S-waves used. In the following we will refer to the results obtained with the $(\pi\pi)$ S-wave from [36] as it requires less free parameters in the fit. The corresponding phase motion is compared in Fig. 4 with the $\pi\,\pi \to \pi\,\pi$ scattering data, averaged from [37].

The $(\pi\pi)$ P-wave was parametrized by the $\rho(770)$ Breit-Wigner function, while for the $\rho\sigma$ state coming from the $^3S_1$ and $^1P_1$ initial states, we found necessary to include in the $(\pi\pi)$ P-wave also the $\rho(1450)$ to improve the fit quality. In this case we describe the $\rho(770)$ and its first radial excitation $\rho(1450)$ in the same partial wave by means of the two-pole K-matrix of (16). Since the $\rho(1700)$ state is very far from the phase-space available for our 4π channel, it was neglected in our analysis.

The F_k pole of (16) corresponding to the $\rho(1450)$ is found at a mass $M = (1.360 \pm 0.010)$ GeV/c^2 and width $\Gamma = (0.270 \pm 0.020)$ GeV/c^2. These values are lower than the nominal mass and width values quoted for this resonance, but they result in full agreement with the weighted average of the world data for the $\rho(1450) \to \pi\pi$ decay: $M = (1.376 \pm 0.007)$ and $\Gamma = (0.290 \pm 0.008)$ GeV/c^2 [11]. The use of different $(\pi\pi)$ S-wave descriptions does not change significantly the low best fit value of the ρ' mass. This result could be due to the rescattering of the ρ' daughter pions with the other two spectator pions, that the symmetrized decay amplitudes based on the isobar model do not take into account [38].

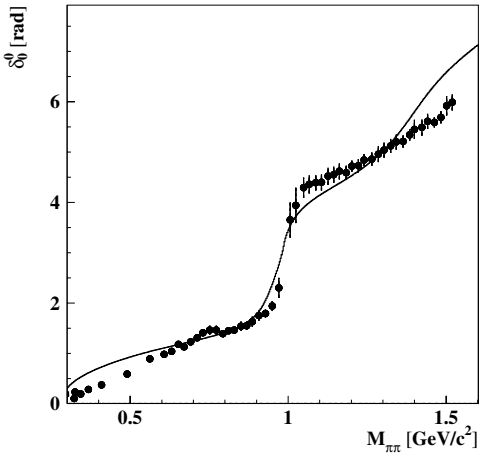

Fig. 4. $\pi\pi$ S-wave amplitude phase motion (solid line) compared to the data from [37]

For the resonances decaying into 3 pions through $\rho\pi$ or $\sigma\pi$ we have considered the following well established states: $a_2(1320)$, $a_1(1260)$ and $\pi(1300)$. Of these three mesons,

only the relatively narrow $a_2(1320)$ reveals a clearly visible peak in the 3π invariant mass distributions (see Fig. 3).

We use the $a_2(1320)$ mass and width from the particle data book [11], since they are known with rather good accuracy. For the $a_1(1260)$ meson we use the values $M = 1.230$ GeV/c^2 and width $\Gamma = 0.400$ GeV/c^2 from [11], or we leave these parameters free in the fit; the best fit result is obtained with $M = 1.330 \pm 0.024$ GeV/c^2 and $\Gamma = 0.580 \pm 0.041$ GeV/c^2, a mass value in close agreement with the CLEO results [39].

We cannot exclude that the large width observed for this meson is due to the interference with the heavier $a_1(1640)$, which is at the limit of our phase space. There is tentative evidence for this meson in the $\tau \to \nu_\tau 3\pi$ decay [39, 40] and, more recently, its existence has been suggested in the analysis of the $\bar{p}p \to 4\pi^0$ reaction in flight [41] and of the $\bar{p}p \to \omega 3\pi^0$ annihilation at rest [42]. Therefore, if this effect is present in the data, our broad a_1 can be regarded only as an effective parametrization of the 1^{++} amplitude.

The fit assigns a negligible percentage to the a_1 decay in $\sigma\pi$:

$$\frac{\Gamma(a_1 \to \sigma\pi)}{\Gamma(a_1 \to \rho\pi)} = 0.06 \pm 0.05 \ , \qquad (20)$$

in agreement with the previous results [11].

For the $\pi(1300)$ meson the best fit gives $M = 1.200 \pm 0.040$ GeV/c^2 and $\Gamma = 0.470 \pm 0.120$ GeV/c^2. By using (14) we find the $\pi(1300)$ decay branching ratio

$$\frac{\Gamma(\pi(1300) \to \sigma\pi)}{\Gamma(\pi(1300) \to \rho\pi)} = 2.2 \pm 0.4 \ , \qquad (21)$$

a value not in good agreement with our previous result of 5.2 ± 0.7 [8] but in full agreement with the old analysis of Aaron and Longacre on the three-pion systems produced in the $\pi^- + p \to (3\pi) + p$ and $\pi^- + p \to (3\pi) + p$ reactions [43]. However, we note that a recent spin-parity analysis of the $\bar{p}d \to \pi^- 4\pi^0 p_{\rm spectator}$ reaction gives a completely different value < 0.15 for this ratio [44].

Also the presence of the exotic $J^{PC} = 1^{-+}$ $\pi_1(1400)$ state proceeding through the $\rho\pi$ decay has been investigated. When the 1^{-+} production is included it improves sensibly the fit, under many different conditions: with different $(\pi\pi)$ S-wave and P-wave parametrizations, with the a_1 and $\pi(1300)$ mass and width values left free or fixed to the mean values of [11], with the annihilation fractions from antiprotonic atom sublevels fixed (fit A and C) or considered as free parameters varying with the target pressure (fit B and D).

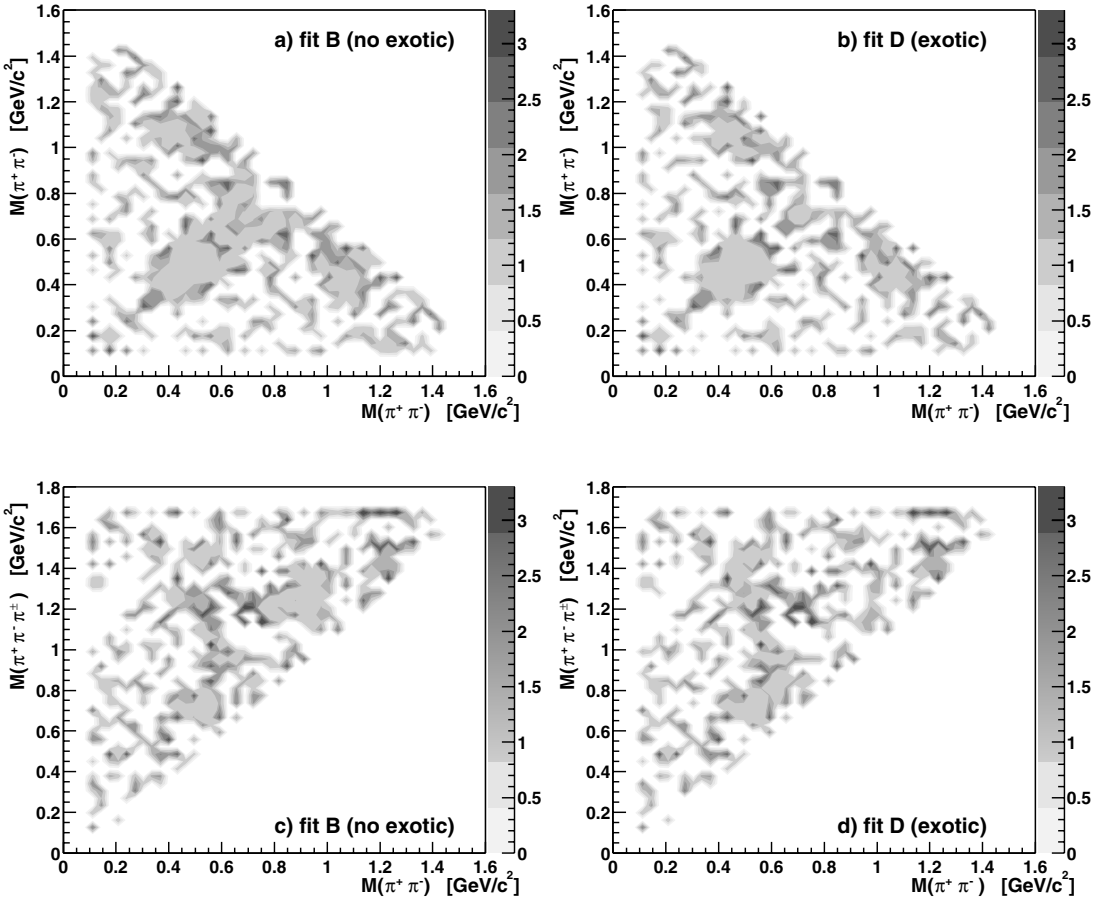

Fig. 5. Absolute differences (in standard deviation units) between the bidimensional invariant mass distributions from fits B and D (see the text) and the gas target data (3 bar pressure). For clarity the differences < 1 are set to zero. The number of combinations per event is as in Fig.2

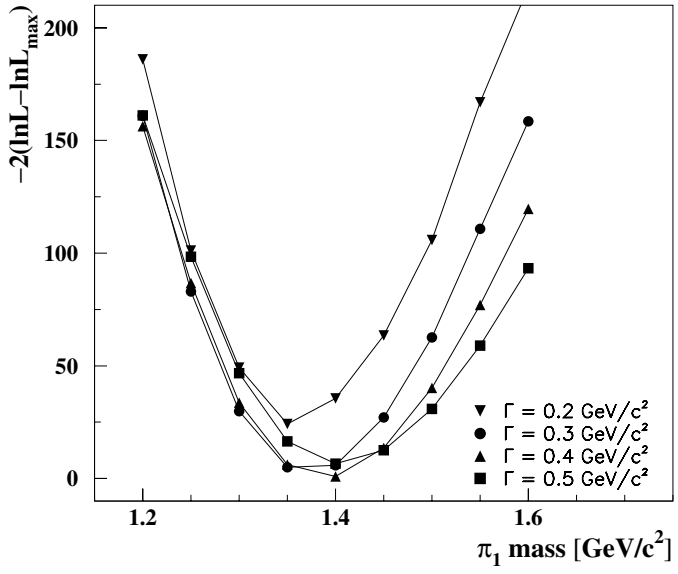

Fig. 6. Dependence of $(-2\ln\mathcal{L})$ on π_1 mass for the set of π_1 width values

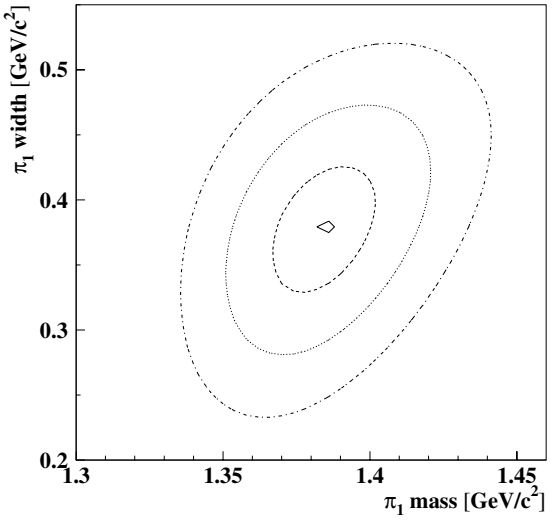

Fig. 7. 1σ,2σ and 3σ error ellipses for the estimate of the π_1 mass and width from the value of $\ln\mathcal{L}$

It is also important to note that the fit results for the masses and widths of a_1 and $\pi(1300)$ do not change significantly also when the π_1 contribution is considered.

The improvement in the fit due to the 1^{-+} contribution can be seen in Table 4 where the fits A and C (A–C) and the fits B and D (B–D) are compared. Since a unit change in our likelihood corresponds to one standard deviation for one degree of freedom, a five standard deviation improvement corresponds, in Table 4, to a $\Delta(-2\ln\mathcal{L})$ change of $\simeq 50$ for each data set (in flight, liquid and gas). Therefore, we deduce that the introduction of the exotic gives a definitive improvement in the data description. Since the absence of the exotic in the $^3P_1$ amplitude is compensated by an increase in the a_1 and a_2 production (see Tables 2 and 3), we observe only slight improvements in the scatter plots after the inclusion of the exotic. However, the improvement is present in *all* the spectra, with the best evidence from the gas data (see Fig. 5). In particular, by comparing Figs. 5c and d, one sees a significant improvement in the $M(\pi^+\pi^-\pi^\pm)$ invariant mass spectra around the π_1 mass.

As a further check, we verified that the introduction of a non-exotic state with $J^{PC} = 1^{+-}$ and mass around 1.4 GeV/c^2 does not improve the fit quality, since in this case $\Delta(-2\ln\mathcal{L}) < 10$ for all the three data sets.

Table 4. Changes in the log likelihood $\Delta(-2\ln\mathcal{L})$ when the 1^{-+} exotic is removed and the remaining contributions are re-optimized in the case of fixed (A–C) and free (B–D) S and P atomic sublevel fractions

fits	flight	liquid	gas	total
A–C	180	142	100	442
B–D	181	160	101	422

We tried different fits, creating a grid of mass values for the exotic with steps of 50 MeV/c^2 and evaluating the fits on the basis of the difference in $\Delta(-2\ln\mathcal{L})$. The behaviour of $(-2\ln\mathcal{L})$ as a function of the π_1 mass value is shown in Fig. 6, and the minimum of $-2\ln\mathcal{L}$ obtained by varying both the π_1 mass and width is shown in Fig. 7. The best estimate of the π_1 parameters is

$$M = 1.384 \pm 0.020\ (\text{stat}) \pm 0.035\ (\text{sys})\ \text{GeV/c}^2 \quad (22)$$
$$\Gamma = 0.378 \pm 0.050\ (\text{stat}) \pm 0.050\ (\text{sys})\ \text{GeV/c}^2\ ,$$

where the systematic errors (written as $\pm\Delta/2$, 100% coverage) have been found by varying the $a_1(1260)$ and $\pi(1300)$ parameters within their PDG confidence intervals and considering the shift of our best fit $\rho(1450)$ mass with respect to the PDG value. This result is in agreement with the present π_1 world data [11].

The exotic meson is produced mainly from the $^1S_0$ and $^3P_1$ initial states, with a dominant production from the $^3P_1$ one, which is the only triplet state where there is no orbital angular momentum between the produced π_1 and the recoiling π ($L = 0$ in Table 1). The inclusion of the π_1 production from this state gives best fit values for the a_1 and a_2 production consistent with zero (see Table 3). If these two mesons are excluded from the $^3P_1$ state, the π_1 production increases from $(47.1 \pm 5.2)\%$ up to $(53.5 \pm 5.3)\%$ with a negligible likelihood decrease. The difference between these two percentages can be considered as an estimate of the systematic error of the analysis.

To check whether the π_1 presence could mimic possible effects due to the apparatus acceptance, we repeated the fit D without the in flight data. All the resulting intermediate state percentages have uncertainties very similar and are in agreement within errors to the data reported in Table 3. The π_1 fractions without the in flight data, for the $^1S_0$, $^3S_1$, $^1P_1$, $^3P_1$ waves are 6.9 ± 1.2, 1.1 ± 0.3, 21.8 ± 8.2 and 44.1 ± 5.7 respectively, to be compared with the data of Table 3. The larger difference is observed in the $^1P_1$

Table 5. Enhancement factor ratios $E_J(\mathrm{LH2})/E_J(\mathrm{gas})$ defined in (19) from fit D compared to some recent analyses of $\bar{p}p$ branching ratios. The data from [2] are the minimum and maximum values depending on different potential models

$^1S_0$	$^3S_1$	$^1P_1$	$^3P_0$	$^3P_1$	$^3P_2$	reference
1.00 ± 0.16	0.91 ± 0.14	0.59 ± 0.29	3.05 ± 0.55	3.34 ± 0.74	1.20 ± 0.20	this work
1.02 ± 0.09	1.00 ± 0.03	0.42 ± 0.32	1.30 ± 0.30	2.43 ± 1.00	0.71 ± 0.10	fit L of [4]
1.02 ± 0.10	0.99 ± 0.04	0.31 ± 0.31	2.61 ± 0.17	1.50 ± 0.63	0.64 ± 0.19	fit H of [4]
$1.03 \div 1.05$	$0.98 \div 0.99$	$0.82 \div 0.97$	$1.60 \div 2.13$	$0.59 \div 0.77$	$0.94 \div 1.06$	[2]

wave, which has a low total intensity and percentages with large errors.

The total π_1 production rate remains stable with or without the in flight data and is about $(4.0 \pm 0.5)\%$ both in LH2 and in gas. A similar production rate was previously observed in the $\pi_1 \to \eta\pi^0$ decay mode by the Crystal Barrel Collaboration [15] in the $\bar{p}p \to \pi^0\pi^0\eta$ annihilation channel. Taking into account that in LH2 at rest the annihilation frequency (3) is an order of magnitude higher than that of $\bar{p}p \to \pi^0\pi^0\eta$ ($(6.7 \pm 1.2) \cdot 10^{-3}$ [33], $(6.5 \pm 0.7) \cdot 10^{-3}$ [45]) one can roughly estimate that $\Gamma(\pi_1 \to \rho\pi)$ is an order of magnitude greater than $\Gamma(\pi_1 \to \eta\pi)$.

The annihilation fractions from the $\bar{p}p$ atomic sublevels P_J of (18), reported in Tables 2 and 3, depend on the target density (liquid or gas). From (19) it results that the ratio

$$\frac{P_J(\mathrm{LH2})B_{4\pi}(\mathrm{LH2})f_J(\mathrm{gas})}{P_J(\mathrm{gas})B_{4\pi}(\mathrm{gas})f_J(\mathrm{LH2})} = \frac{E_J(\mathrm{LH2})}{E_J(\mathrm{gas})}$$

is independent of the weights g_J and of the hadronic branching ratios B_J and gives the enhancement factor ratios. For the S and P-waves percentages $f_J(\delta)$ we use in liquid the values $f_S(\mathrm{LH2}) = (0.868 \pm 0.010)$ when $J = {}^1S_0, {}^3S_1$ and $f_P(\mathrm{LH2}) = (0.132 \pm 0.010)$ when $J = {}^1P_1, {}^3P_0, {}^3P_1, {}^3P_2$; for a 3 bar pressure gas we use the values $f_S(\mathrm{gas}) = (0.435 \pm 0.010)$ and $f_P(\mathrm{gas}) = (0.565 \pm 0.015)$, obtained interpolating between the NTP and 15 bar pressure values [2–4]. From the results of Tables 2 and 3, it is then possible to obtain directly the ratio of the enhancement factors and to compare them with some predictions. As previously noted in Sect. 2, for the gas target data the comparison is meaningful within 5%, in spite of the different target pressures.

The results are shown in Table 5. The ratios of [4] reported as fit L and fit H have been obtained with the use of the low ($(2.61 \pm 0.24)\, 10^{-4}$) and high ($(6.93 \pm 0.43)\, 10^{-4}$) values measured for the $\bar{p} \to \pi^0\pi^0$ reaction branching ratio in liquid. We refer to [3,4,25] for the references and a detailed discussion on these two incompatible experimental values.

From the table we see, in full agreement with the previous analyses [2–4], that the $^1S_0$ and $^3S_1$ protonium populations have enhancement factors equal to one, so that at any density we have the statistical ratio 3:1 for triplet/singlet. The situation for the P-levels is less clear: the $^3P_1$ state appears enhanced in liquid in contrast with the predictions of [2] and in closer agreement with the fit L of [4] and also with our coupled channel analysis [46]; on the other hand, the enhancement of the $^3P_0$ state in liquid seems closer to the prediction of [2] and of the fit H of [4]. In the other cases the large errors prevent more definitive conclusions.

Finally, we note that the total annihilation percentages from P and S-waves in Tables 2 and 3 are more or less the same for the different fits and that the global P-wave annihilation percentages are higher than the P-wave atomic population fractions, that are $\simeq$ 10–14% in LH2 and $\simeq$ 57–59% in NTP gas. [2–4].

5 Conclusions

A total of 90 000 $\bar{p}p \to 2\pi^+2\pi^-$ annihilation events, equally divided in annihilation at rest in liquid hydrogen, at rest in gaseous hydrogen (3 bar pressure) and in flight at very low $\bar{p}$ momentum ($\simeq$ 50 MeV/c) have been analyzed.

Assuming that the annihilation fraction values vary as a function of the target density, we obtain that the annihilations from the $^3P_0$ and $^3P_1$ states are enhanced in liquid with respect to the gaseous target, in qualitative agreement with other analyses [2–4].

A good fit has been obtained introducing all the decay channels listed in Table 1, where the masses, widths and branching ratios of some resonances have been studied.

In particular for the $\pi(1300)$ mass and width we find $M = 1.200 \pm 0.040$ GeV/c^2 and $\Gamma = 0.470 \pm 0.120$ GeV/c^2, with a preferred decay mode into $\sigma\pi$ (2.2 ± 0.4 times the $\rho\pi$ one, see (21)), not in good agreement with the value 5.2 ± 0.7 of our previous work [8]. The overall production of this meson both in liquid and in gas amounts to about 2%.

The fit assigns to the $a_1(1260)$ the values $M = 1.330 \pm 0.024$ GeV/c^2 and $\Gamma = 0.580 \pm 0.041$ GeV/c^2, with a dominant decay mode into $\rho\pi$ (see (20)).

The fit improves with the inclusion of a $\rho(1450)$ state with a preferred mass around 1.36 ± 0.01 GeV/c^2, a low value typical of all the analyses of the $\rho(1450) \to \pi\pi$ decay [11,46]. However, we note that our results on the other resonances discussed in this paper hold even if we fix the ρ' mass at the standard value $M = 1.452$ GeV/c^2.

The possible $\rho\pi$ decay of the $\pi_1(1400)$ meson, with exotic quantum numbers $J^{PC} = 1^{-+}$ has been studied for the first time. The introduction of this resonant P-wave gives a not negligible improvement to the fit and its contribution is independent of the adopted $(\pi\pi)$ S-wave

and of the ρ', a_1 and $\pi(1300)$ mass values. Within the limits of the present data accuracy we can affirm that the decay to $\rho\pi$ is about one order of magnitude greater than the previously studied decay mode to $\eta\pi$ [12–15].

An isovector resonance with quantum numbers $J^{PC} = 1^{-+}$ is neither a $\bar{q}q$ state nor a glueball. Our observation of this wave also in the $\bar{p}p \to 4\pi$ channel, with mass and width values (22), in agreement with those found in the $\bar{p}p \to \eta\pi\pi$ channel [14,15], seems to exclude the hypothesis of an artifact of the spin-parity analyses and supports the existence of a $(q\bar{q}g)$ hybrid or a $(q^2\bar{q}^2)$ four-quark state meson [47].

A ground state hybrid is expected to have an appreciably larger $\rho\pi$ width than $\eta\pi$ width [48] and, according to some models, its existence could imply that the $\pi(1300)$ pion is predominantly a hybrid meson with a large $\sigma\pi$ branching fraction [49]. Both these predictions are in agreement with the analysis presented here.

On the other hand, most of models predict the hybrid lowest mass around 1.6 GeV/c^2 [48,50] and, in the constituent quark-gluon model, the hybrid cannot decay in $\eta\pi$ and $\eta'\pi$ [51]. However, the $\eta\pi$ decay is allowed if one consider the $\pi_1(1400)$ meson as a four-quark state belonging to the $\mathbf{10} \oplus \overline{\mathbf{10}}$ representation with allowed coupling to two octet states [52]; in this framework, the decay to $\rho\pi$ can be explained with s-channel loop diagrams containing the intermediate states $\rho\pi$, $\eta\pi$ and $K^*\bar{K} + \bar{K}^*K$ [53].

To discriminate between these two hypotheses, new data on π_1 production with hadronic and electromagnetic probes are probably necessary.

Appendix: Angular distributions in the decay $\bar{p}p \to 2\pi^+2\pi^-$

The angular distributions of the final state in the decay $\bar{p}p \to 2\pi^+2\pi^-$ are evaluated by means of covariant spin tensor amplitudes as explained in [27] and the results obtained are identical to those given by the covariant helicity formalism of [28]. These amplitudes are evaluated in terms of the elementary spin tensors which describe both the intrinsic spin j and the relative orbital angular momenta L of the involved resonances for decays of the type $J \to j + L$. This formalism has been extensively used in other analyses of the Obelix Collaboration in the framework of the isobar model.

For the specific case of this paper, the decay channel $\bar{p}p \to \rho\rho$ occurs from different initial states as reported in Table 1 and for the $^1S_0$ state the selection rules impose a configuration of angular momenta and spins such as $j_1 = 1$, $j_2 = 1$, $L = 1$ and $J = 0$. Hence, it has been necessary to extend the spin tensor formalism to describe the case of two spin-1 resonances with an orbital angular momentum different from zero to include the $\rho\rho$ channel, which is a decay of the type $J \to 1^- + 1^- + L$. In this appendix we outline the calculation of this amplitude in the framework of the covariant spin tensor formalism [27].

We indicate the four-momenta of the 4 pions in the center of mass reference system with the letters a, b, c and d, the four-velocities of the two resonances with w_1^μ and w_2^μ and the initial state four-velocity with u^μ:

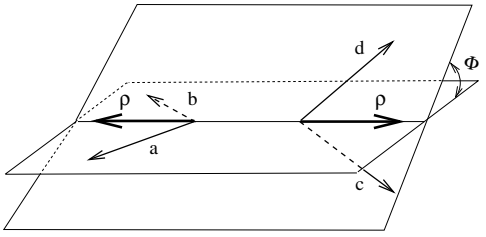

Fig. 8. Angles used in the description of the $\bar{p}p \to \rho\rho \to 2\pi^+\,2\pi^-$ reaction. The pion momenta are labeled with a, b, c, d

$$u^\mu = (a + b + c + d)^\mu / s$$
$$w_1^\mu = (a + b)^\mu / (a + b)^2$$
$$w_2^\mu = (c + d)^\mu / (c + d)^2 \ .$$

If S_1 and S_2 are the two ρ spin tensors associated to the two spins j_1 and j_2 and L is their relative orbital angular momentum, we can write:

$$S_1^\mu = (a - b)^\mu - w_1^\mu (m_a^2 - m_b^2)$$
$$S_2^\mu = (c - d)^\mu - w_2^\mu (m_c^2 - m_d^2)$$
$$L^\mu = [(c + d) - (a + b)]^\mu - u^\mu (m_{\rho_1}^2 - m_{\rho_2}^2) \ ,$$

where m_{ρ_i} is the invariant mass of the i-th resonance. By using one of the spin projectors Θ of [27], the decay amplitude for the decay $0 \to 1 + 1 + 1$ is evaluated as:

$$A = \epsilon_{\mu\nu\rho\sigma} S_1^\mu S_2^\nu L^\rho u^\sigma \ ,$$

where $\epsilon_{\mu\nu\rho\sigma}$ is the Levi-Civita tensor.

This formula corresponds to the LS scheme where the spin amplitude is calculated in two steps: first S_1 and S_2 are summed to give the total spin S and then L is summed to S to give the initial spin J; the calculation is performed in the $\bar{p}p$ reference system in a totally covariant way.

The probability computed by squaring A gives the final state angular distribution and the result is expressed as a function of some selected kinematical variables.

By defining the Φ angle in the center of mass as (see also Fig. 8):

$$\cos\Phi = \frac{(\mathbf{a} \times \mathbf{b}) \cdot (\mathbf{c} \times \mathbf{d})}{|\mathbf{a} \times \mathbf{b}||\mathbf{c} \times \mathbf{d}|}$$

and the angles θ_1 in the first resonance reference frame (indicated by the primes) and θ_2 in the second resonance reference frame (indicated with double primes) as:

$$\cos\theta_1 = \frac{\mathbf{a}' \cdot (\mathbf{c}' + \mathbf{d}')}{|\mathbf{a}'||\mathbf{c}' + \mathbf{d}'|}$$
$$\cos\theta_2 = \frac{\mathbf{c}'' \cdot (\mathbf{a}'' + \mathbf{b}'')}{|\mathbf{c}''||\mathbf{a}'' + \mathbf{b}''|} \ ,$$

it is possible to show that the decay probability for the channel $(\rho\rho)_{L=1}$ is given by:

$$P = |A|^2 = \sin\theta_1{}^2 \sin\theta_2{}^2 \sin\Phi^2 \ .$$

This result is in analytical and numerical agreement with the one obtained by using the helicity-coupling formalism of [28] applied to this decay channel.

References

1. J.Diaz et al., Nucl. Phys. B **16**, 239 (1970).
2. C.Batty, Nucl. Phys. A **601**, 425 (1996).
3. Obelix Collaboration, G.Bendiscioli et al., Nucl. Phys. A **686**, 317 (2001).
4. P.Salvini et al., Nucl. Phys. A **696**, 527 (2001).
5. Obelix Collaboration, A. Zenoni et al., Phys. Lett. B **461**, 405 (1999).
6. J.Carbonell, K.Protasov, Z. Phys. A **355**, 87 (1996).
7. J.Carbonell et al., Phys. Lett. B **397**, 345 (1997).
8. Obelix Collaboration, A.Bertin et al., Phys. Lett. B **414**, 220 (1997).
9. P.Salvini, Proceedings of the Fifth Biennal Conference on the Low Energy Antiproton Physics, LEAP'98, edited by C. Cicaló et al, Nucl. Phys. A **655**, 51c (1999).
10. P.Salvini, Proceedings of the Sixth Biennal Conference on the Low Energy Antiproton Physics, LEAP'00, edited by W. Dünnweber et al, Nucl. Phys. A **692**, 340c (2001).
11. Review of Particle Physics, Phys. Rev. D **66**, 1 (2002).
12. E852 Collaboration, D.R. Thompson et al., Phys. Rev. Lett. **79**, 1630 (1997).
13. E852 Collaboration, S.U.Chung et al., Phys. Rev. D **60**, 092001 (1999).
14. Crystal Barrel Collaboration, A.Abele et al., Phys. Lett. B **423**, 175 (1998).
15. Crystal Barrel Collaboration, A.Abele et al., Phys. Lett. B **446**, 349 (1999)
16. T.Barnes et al., Phys. Rev. D **55**, 4157 (1997).
17. Obelix Collaboration, M.Agnello et al., Phys. Lett. B **256**, 349 (1991).
18. Obelix Collaboration, A.Bertin et al., Phys. Lett. B **369**, 77 (1996).
19. Obelix Collaboration, A.Adamo et al., Phys. Lett. B **287**, 368 (1992).
20. F.Balestra et al., Nucl. Instr. Meth. A **323**, 523 (1992).
21. Obelix Collaboration, A.Adamo et al., Sov. J. Nucl. Phys. **55**, 1732 (1992).
22. C.Baltay et al., Phys. Rev. **145**, 1103 (1966).
23. M. Cresti et al., in Proceedings of the Siena International Conference on Elementary Particles and high-energy physics, Siena, Italy, 1963, edited by G.Bernardini, G.P.Puppi, Società Italiana di Fisica, Bologna, (1963).
24. Asterix Collaboration, M. Doser et al., Phys. Lett. B **215**, 792 (1988).
25. Crystal Barrel Collaboration, A. Abele et al, Nucl. Phys. A **679**, 563 (2001).
26. Obelix Collaboration, A.Bertin et al., Phys. Rev. D **57** 55 (1998); A.Fontana, Ph.D.Thesis, University of Pavia (unpublished), 1997
27. V.Filippini et al., Phys. Rev. D **51**, 2247 (1995).
28. S.U.Chung et al., Phys. Rev. D **48**, 1225 (1993).
29. S.U.Chung et al., Ann.Physik. **4**, 404 (1995).
30. F.v. Hippel, C.Quigg, Phys. Rev. **5**, 624 (1972).
31. S.M. Flatté, Phys. Lett. B **63**, 224 (1976).
32. V.V. Anisovich et al., Phys.Rev. D **50**, 1972 (1994).
33. Crystal Barrel Collaboration, C. Amsler et al., Phys Lett. B **333**, 227 (1994).
34. F.James et al., MINUIT, CERN-Report CERN-DD D506.
35. V.V. Anisovich et al., Phys. Lett B **389**, 388 (1996).
36. Obelix Collaboration, A. Bertin et al., Phys. Lett. B **408**, 476 (1997).
37. G. Grayer et al., Nucl. Phys. B **75**, 189 (1974).
38. Crystal Barrel Collaboration, A. Abele et al., Phys. Lett. B **469**, 270 (1999).
39. CLEO Collaboration, D.M.Asner et al., Phys. Rev. D **61**, 012002 (2000).
40. DELPHI Collaboration, P. Abreu et al., Phys. Lett B **426**, 411 (1998).
41. C.A. Baker et al., Phys. Lett B **449**, 114 (1999).
42. C.A. Baker et al., Phys. Lett B **563**, 140 (2003).
43. R.A Aaron, R.S. Longacre, Phys. Rev. D **24**, 1207 (1981).
44. Crystal Barrel Collaboration, A. Abele et al., Eur. Phys. J. C **19**, 667 (2001).
45. Crystal Barrel Collaboration, C. Amsler et al., Phys. Lett. B **322**, 431 (1994).
46. Obelix Collaboration, M. Bargiotti et al., Eur. Phys. J. C **26**, 371 (2003).
47. C. Amsler, Rev. of Mod. Phys. **70**, 1293 (1998).
48. A. Donnachie, P.R. Page, Phys. Rev. D **58** 114012 (1998).
49. A. Donnachie, Yu.S. Kalashnikova, Phys. Rev. D **60** 114011 (1999)
50. H.Y. Jin et al., Phys. Rev. D **67** 014025 (2003).
51. F. Iddir, A.S. Safir, Phys. Lett. B **507**, 183 (2001).
52. S.U. Chung et al., Eur. Phys. J. A **15**, 539 (2002).
53. N.N. Achasov, G.N. Shestakov, Phys. Rev. D **63**, (2000).